doi:10.2533/chimia.2022.570 Chimia 76 (2022) 570–574

Control of the Two-photon Visual Process in *ex vivo* Retinas and in Living Mice

Geoffrey Gaulier[a], Quentin Dietschi[b], Aleksa Djorovic[a], Luca La Volpe[a], Tania Rodrigues[a], Luigi Bonacina[a], Ivan Rodriguez[b], Jean-Pierre Wolf[a]*

Abstract: Palcewska *et al*. first demonstrated near infrared (NIR) visual response in human volunteers upon two-photon absorption (TPA), in a seminal work of 2014, and assessed the process in terms of wavelength- and power-dependence on murine *ex vivo* retinas. In the present study, *ex vivo* electroretinography (ERG) is further developed to perform a complete characterization of the effect of NIR pulse duration, energy, and focal spot size on the response. The same set of measurements is successively tested on living mice. We discuss how the nonlinear intensity dependence of the photon absorption process is transferred to the amplitude of the visual response acquired by ERG. Finally, we show that the manipulation of the spectral phase of NIR pulses can be translated to predictable change in the two-photon induced response under physiological excitation conditions.

Keywords: Rhodopsin · Two-photon absorption · Visual process · Electroretinography · Femtosecond pulse-shaping

Introduction

The vision process relies on the photo-activation of rods and cones. Upon photon absorption, the retinal moiety of visual receptors changes its conformation, triggering a sequence of events culminating with the generation of an electric signal to the brain.[1–3] Human visual perception spans from 400 to 720 nm,[4] while the spectral sensitivity of mice is shifted to the ultraviolet.[5] Recently, we have studied the effect of spectral phase of green ultrafast pulses on the visual response of living mice.[6] In parallel, we have witnessed a series of experiments demonstrating approaches for widening the range of wavelengths that can be perceived by a species beyond the natural response of its photoreceptors. For instance, Ma *et al*. used lanthanide-doped nanoparticles in direct contact with the retina of living mice to upconvert NIR (980 nm) to green (535 nm) light.[7] An alternative approach to extend the range of perceived wavelengths, which does not require the use of exogenous agents, is based on the nonlinear absorption of NIR photons, usually generated by a short-pulse laser source. This has been demonstrated on *ex vivo* murine retina[4,8] and on human volunteers.[4,9–13] In this work, we pursue this approach complementing *ex vivo* and *in vivo* measurements on mice, highlighting the dependence of the visual response on several excitation parameters (energy, size, and duration of the pulse), and we also show that the two-photon induced response can be modulated by the spectral phase of the light pulses under physiological excitation conditions. For all the experiments presented, the main observable is the electro-physiological signal emitted by the retina acquired by electroretinography (ERG). This signal shows two different characteristics: a hyperpolarization called A-wave, and a successive depolarization called B-wave (Fig. 1.A, inset). The A-wave originates from the photoreceptors, emitted after the biological processes following the isomerization of rhodopsin, while the B-wave originates from bipolars cells, initiated by the hyperpolarization of the photo-receptors.[2]

1. Methods

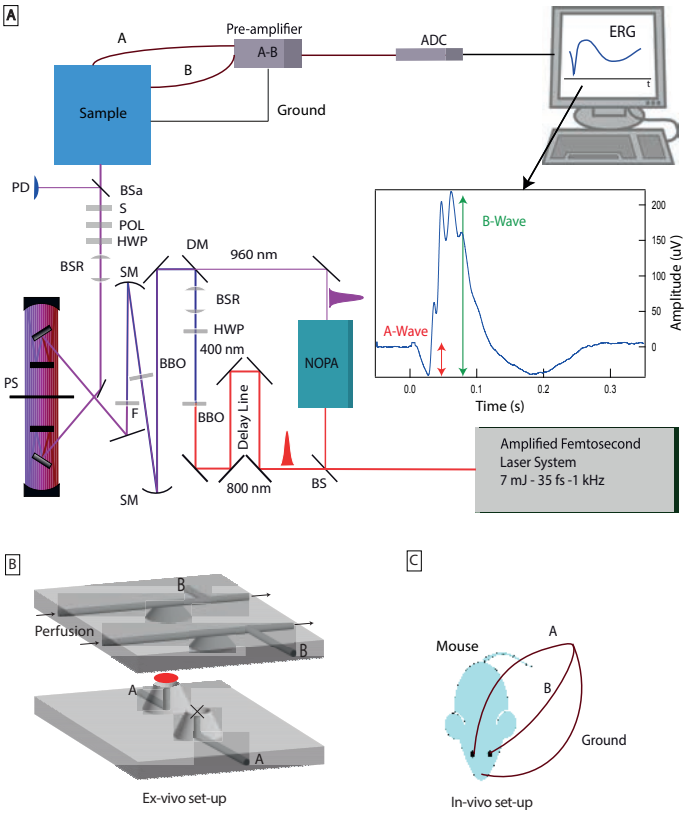

Fig. 1. A. Experimental setup. BS: Beamsplitter, NOPA: Noncollinear Optical Parametric Amplifier; SM: Spherical Mirror f = 2 m; BBO: Beta Barium Borate crystal (cutting angle for both: 29.2°, Thickness 2 mm, Eksma Optics); F: Longpass filter (FELH800 - Thorlabs); DM: Dichroic Mirror; HWP: Half Wave Plate; POL: Polarizer; S: Beam shutter; PS: Pulse shaper in a 4-f line; BSR: Beam Size Reducer Lens Assembly (f_1 = 50 cm and f_2 = -20 cm); ADC: Analog to Digital Convertor; PD: Photodiode; ERG: Electroretinogram. B. *Ex vivo* sample holder for ex-vivo measurements. The retina is placed at the location indicated by the red circle with photoreceptors facing up. C. *In vivo* measurement configuration.

*Correspondence: [a]Group of Applied Physics, University of Geneva, 22 Ch. de Pinchat, 1211 Geneva, Switzerland
[b]Department of Genetics and Evolution, University of Geneva, 30 Quai Ansermet, 1211 Geneva, Switzerland *Jean-Pierre.Wolf@unige.ch

The experimental set-up is reported in Fig. 1.A. The output from a 1 kHz Ti:Sapphire amplifier (Astrella, Coherent Inc.) is split into two pulse trains. The first one is frequency converted by a nonlinear optical parametric amplifier (TOPAS-White, Light Conversion) to produce 7 μJ, 80 fs pulses at 960 nm. An additional home-made OPA stage[14, 15] pumped by the second pulse train is introduced to increase the output energy up to 40 μJ (120 fs pulse duration). The need of this amplification stage is mainly determined by the losses introduced by the gratings used for the 4*f* zero-dispersion line housing a spatial light modulator (SLM-S640, by Jenoptik) at its Fourier plane, used for acting on the spectral phase of the 960 nm pulses. The beam exiting the 4f-line is collimated and reduced in transverse size down to approximately 2 mm diameter. A fast silicon photodiode (SM05PD28) combined with a gated integrator (SR280 - Stanford Research Systems) monitors pulse energy shot-by-shot. A combination of a half wave plate and a polarizer set on a computer-controlled motorized rotational stage (PRM1/MZ8 - Thorlabs) is used to adjust pulse energy. A fast electronic shutter (Newport model 76992) allows to single out five consecutive pulses from the 1 kHz source to illuminate one eye of the mouse. The full cycle to the next irradiation lasts two seconds.

The *in vivo / ex vivo* system, in Fig. 1.B and Fig. 1.C, respectively, and the signal pre-amplifier (SR560 by Stanford Research System inc., working on battery power) are enclosed in a custom-made Faraday cage to reduce the 50 Hz noise pickup. The analog signal is frequency filtered (between 0.3 and 3000 Hz), amplified by a factor 5000, and digitized by an analog-to digital converter (ADC - PCI-6220 by National Instruments) at 25 kHz sampling rate. During data acquisition, the ERG trace is sampled leaving a few milliseconds before and after each illumination event.

For *in vivo* measurements (Fig. 1.C), the detection system and the measurement protocol are identical to those described in our previous work.[6] Briefly, 6-8 week-old C57BL/6 male mice are anesthesized using a mix of ketamine/xylazine as described in ref. [6] The beam illuminates the right eye, while the electro-physiological potentials are acquired from both eyes using contact lens electrodes (Ocuscience). The two electrodes are connected to the differential amplifier.

For *ex vivo* experiments (Fig. 1.B), the eye is carefully pulled out of the orbit, cut from the optic nerve and placed in cold sterile Ames' medium (Sigma Aldrich) prepared according to manufacturer's instructions. The retina is dissected from the other eye tissues and placed, photoreceptors facing up, on a commercial holder (OcuScience)[16] at the sample position in Fig. 1.A. The signal is acquired via an electrode embedded in a bath of electrolyte solution (NaCl 140 mM, KCl 3.6 mM, $MgCl_2$ 2.4 mM, $CaCl_2$ 1.2 mM, HEPES 3.0 mM and EDTA 0.01 mM) in contact with the bottom of the retina (ganglion cell layer side). The other electrode is connected to the perfusion (Ames' medium heated at 37°C, oxygenated using a 95%/5% CO^2/ O^2), which flows at 50 mL/hour. The *ex vivo* signal is further filtered by a 50 Hz notch filter (2355-50-BNC by KR electronics, Inc). Note that the measurement performed requires only one retina, therefore the second dome on the holder is not used.

2. Visual Response *ex vivo*

For a precise study of TPA-induced vision, the *ex vivo* approach is ideal, as it presents the advantage of working without the lens (thickness: 1.6 mm[17]) in the beam path. This helps reducing uncertainties in the intensity values, as in the near infrared the optical and spectroscopic characteristics of the mouse eye are not well established.[18, 19] Aside from absorption, the lens could also affect pulse intensity at the retina by temporal pulse stretching. In our experiment, we successfully measured the B-wave amplitude as a function of three distinct excitation parameters: pulse energy, pulse duration, and beam diameter. The results are shown in Fig. 2.

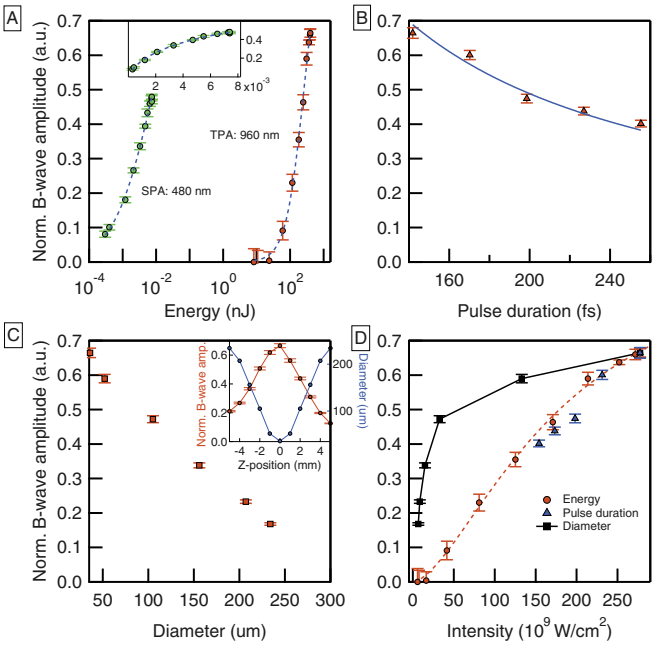

Fig. 2. *Ex vivo* characterization of the retinal response. A: Normalized B-wave response upon 480 nm (green dots) and upon 960 nm (red dots) excitation. Blue lines: Naka-Ruhston equation fittings. Inset: Normalized B-wave amplitude response upon 480 nm using a linear scale. B: Normalized B-wave amplitude as a function of the pulse duration. Blue lines: fit of f(Δt)= a/Δt. C: Normalized B-wave amplitude as a function of the beam diameter. Inset: Normalized B-wave amplitude as a function of the lens position (red) and beam diameter (blue) as a function of the lens position (Z-position). D: Normalized B-wave amplitude as a function of intensity, plotted for the energy, pulse duration, and diameter dependence. Results in B; C and D are obtained at 960 nm excitation.

The energy curves for SPA and TPA were fitted using the Naka-Rushton equation:[4, 20, 21]

$$f(E) = R_{max}\frac{E^n}{E^n + E_{1/2}^n} \quad (1)$$

R_{max} corresponds to the saturation level, $E_{1/2}$ is the required energy to generate a signal of amplitude $\frac{R_{max}}{2}$ while n relates to the slope in a logarithmic representation. The traces in all plots are normalized with respect to R_{max}. For the energy dependence (Fig. 2.A), the visual response at 960 nm is directly compared to that obtained by single-photon absorption (SPA) at 480 nm. The visible wavelength is obtained by doubling the frequency of the infrared pulse in a nonlinear crystal. We observed that substantially more energy is needed to measure a B-wave at 960 nm than at 480 nm (SPA:8.0 ± 3.1 pJ, TPA: 260 ± 34 nJ).

For pulse duration dependence (Fig. 2.B), we applied a negative chirp using a multi-pass prism compressor (BOA - Swamp Optics), and measured the ERG as a function of the pulse duration of the infrared pulse. The B-wave amplitude decreases as the pulse duration increases at 960 nm. The same trace is plotted in Fig. 2.D as a function of intensity (blue triangles). For the beam diameter dependence (Fig. 2.C), we focused the infrared light using a f = 36 mm lens, and measured the ERG as a function of the lens position. The size of the beam is measured using a beam profiler (Newport, LBP-1-USB).We observed that the B-wave decreases as the beam diameter increases, which is also expected from a multiphoton process depending non-linearly on the excitation intensity. The same trace is also reported in Fig. 2.D (black squares). Note that the beam diameter was kept below 250 um throughout the experiment to ensure that the density of the receptors in

the region probed was sufficiently homogeneous to perform a comparison.

Looking at Fig. 2.A, one can note that the ERG signal does not increase linearly with energy for SPA, and quadratically for TPA. While the SPA follows the typical saturation trend (see inset) already reported [2, 22–25] which can be directly linked to the eye physiological response, the TPA trace requires further considerations. In the following, we rationalize it assuming that the ERG signal is determined by an interplay of two distinct contributions: i) a subpicosecond one, localized at the molecule site and associated with the photon absorption and the isomerization of rhodopsin, followed by ii) a much slower process governed by the physiological response and leading from the isomerized state to the generation of the B-wave . The physiological response is expected to be independent from the photo-excitation mechanism, but it might depend on the number of isomerized molecules. We can model the photo-molecular interaction (i) for SPA and TPA using the rate equations for a two-state model (not taking into account stimulated emission):

$$\text{SPA: } \frac{dN_2}{dt} = \sigma_1 N_1(A) I(A,t) \tag{2}$$

$$\text{TPA: } \frac{dN_2}{dt} = \sigma_2 N_1(A) I(A,t)^2 \tag{3}$$

For SPA, the number of excited molecules N_2 increases linearly with the energy. Assuming homogeneous molecule surface concentration at the retina, $N_1 \propto d^2$. Considering that $I \propto \frac{1}{d^2}$, SPA should be insensitive to the beam diameter. As for all linear processes, we also expect no dependence on pulse duration.

For TPA, the number of excited molecules N_2 increases with the pulse energy at fixed pulse duration quadratically, and taking into account both that $I^2 \propto \frac{1}{d^4}$ and $N_1 \propto d^2$, N_2 should scale as $\frac{1}{d^2}$. Upon integration over the pulse duration, one can also see that $N_2 \propto \frac{1}{\Delta t}$.

In agreement with our assumptions, we observe in Fig. 2.B that the dependence of the TPA signal on the pulse duration is approximated by $\frac{1}{\Delta t}$. We can understand the good agreement with the rate equation of the ultrafast mechanism (i) as the parameter Δt is significant only for the photo-dynamics at short times. On the other hand, the dependence of the ERG signal on the diameter (Fig. 2.C) behaves very differently from $\frac{1}{d^2}$, indicating that the B-wave is modulated by the physiological response which is sensitive to the extent of the excited surface at the retina (see Fig. 2.D).[26]

It is possible to compare the excitation rates for SPA and TPA (Equation 2 and Equation 3), using parameter values found in the literature. The SPA cross-section σ_1 for the cis-ground state can be derived from the molar extinction coefficient of rhodopsin at 500 nm (n = 40200 $cm^{-1}M^{-1}$).[27]

$$\sigma_1 = \ln(10)\frac{10^3}{N_A}\epsilon = 1.5 \cdot 10^{-16}\ \text{cm}^2 \text{ at 500 nm.} \tag{4}$$

The TPA cross-section σ_2 was previously determined by Palczewska *et al.*[4]: $\sigma_2 = 10^{-50}$ cm^4s. The full list of parameters used in the calculations are provided in Table 1. For both SPA and TPA, we used the $E_{1/2}$ value from the Naka-Rushton fit. The intensity is calculated as $I = \frac{\text{Number of photons}}{A \cdot \Delta T}$. Note that this simplified model assumes a square pulse. The rates found for both conditions are very similar: $\sigma_1 I = 2.6 \pm 1.3 \cdot 10^9\ s^{-1}$ and $\sigma_2 I^2 = 1.3 \pm 0.7 \cdot 10^{10}$ $s^{-1}$for SPA and TPA respectively. We assumed an uncertainty of 5 fs on the pulse duration, 5 μm on the diameter and used the error given by the fitting procedure for the energy (SPA: 3.1 pJ and TPA: 34 nJ). We have conducted a simple quantitative comparison at the $E_{1/2}$ positions retrieved on both curves. The corresponding values for $\sigma_1 I$ and $\sigma_2 I^2$ point to the fact that the pulses used in each experiment isomerize approximately the same number of molecules. Following Palczewska *et al.*,[4] we can rule out a SPA contribution from the spectral tail of the 960 nm pulse.

Table 1. Pulses characteristics used in the *ex vivo* experiment.

	SPA	**TPA**
Pulse Duration ΔT (fs)	120 ± 5	120 ± 5
Diameter (μm)	36 ± 5	36 ± 5
Area A(cm^2)	$1.0 \cdot 10^{-5}$	$1.0 \cdot 10^{-5}$
Energy (J)	$8.0 \pm 3.1 \cdot 10^{-12}$	$2.6 \pm 0.34 \cdot 10^{-7}$
Number of Photons	$2.1 \cdot 10^7$	$1.4 \cdot 10^{12}$
$\sigma_1 I$ (s^{-1}) $\sigma_2 I^2$ (s^{-1})	$2.6 \pm 1.3 \cdot 10^9$	$1.3 \pm 0.7 \cdot 10^{10}$

3. Visual Response *in-vivo*

Ex vivo configuration allows for a more precise control of the parameters of the input beam and a better signal to noise ratio due to the absence of heart beat and respiration. However, the retinal pigment epithelium is detached from the retina during *ex vivo* experiments, which impairs renewal of the retinal,[16, 28], and reduces the signal over time. We therefore proceeded in measuring TPA-induced visual response in living mice. We first measured the power dependence of the ERG. The B-wave as a function of the energy for both visible (SPA) and infrared (TPA) femtosecond excitation is displayed in Fig. 3.

In agreement with the *ex vivo* results, the energy necessary to induce an electro-physiological response is of the order of the μJ, for a 120 fs pulse. In the experiment, the beam size at the retina needs to be carefully adjusted, in order to maximize the intensity for the TPA process. This was achieved using a telescope lens arrangement and adjusting the position of the second lens to optimize the ERG amplitude. We notice that the maximum B-wave amplitude in *ex vivo* retinas is smaller than its amplitude in living mice (34 μV, instead of 160 μV for the SPA case). It has been reported that this discrepancy can be addressed by a better sample preparation.[16] We also notice that the energy required to reach the $E_{1/2}$ (SPA: $2 \cdot 10^{-3}$ nJ and 10^{-2} nJ, TPA: 0.180 μJ and 5 μJ for *ex vivo* and *in-vivo* respectively) increases by one order of magnitude as already observed by Vinberg *et. al.*[16]

After determining the excitation parameters for obtaining TPA-induced visual response under physiological conditions *in vivo*, we investigated the sensitivity of the ERG signal to the temporal shape of the infrared femtosecond pulse. We relied on a phase-modulation scheme already applied to atomic and molecular systems.[29–32] The approach consists of scanning a π-phase step throughout the infrared pulse spectrum dispersed in the Fourier plane of a 4-f zero dispersion compressor[33] (see Fig. 1.A, PS) and measuring a signal related to the excitation of an electronic level (by absorption of fluorescence). Note that this optical scheme leaves the photon number (energy) and spectrum unchanged, while the temporal profile (and thus the intensity) of the pulse is modified.

We characterized the performance of our set-up for pulse-shaping by performing the experiment on Rhodamine 6G in ethanol, using the dye fluorescence as an observable, right before and after the in-vivo measurements. The experiment is repeated on

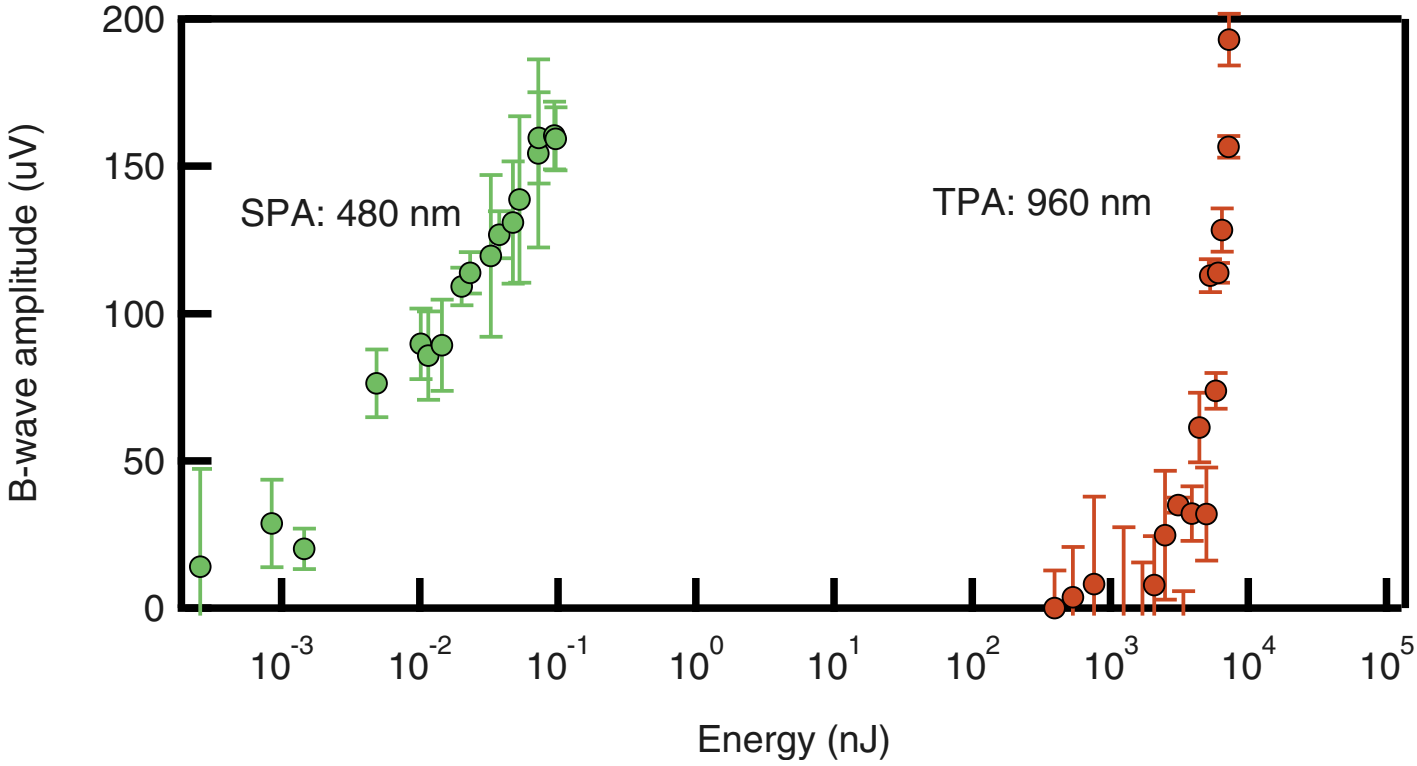

Fig. 3. Amplitude of the B-wave generated upon 480 nm (green dots) and upon 960 nm (red dots) excitation in living mice.

two different animals. An ERG is measured every 2 seconds upon 5 pulse irradiation at 1 kHz. Every 2 ERGs, the π-step is spectrally shifted by a few nm (2.3 and 1.5 for mouse 1 and 2 respectively, corresponding to 10 and 15 pixels on the SLM). The scan is repeated during 45 min, 3 times per mouse (with one anaesthesia every 45 min).The same experiment on rhodamine 6G in ethanol is performed using a two-lens scheme ($f = 3.5$ cm), a filter (BG40, Thorlabs), and a photomultiplier tube (Hamamatsu H7826).

Fig. 4.A shows the experimental laser spectrum centered at 960 nm (dots). In Fig. 4.B we show the calculated temporal profile assuming a positive chirp of 1200 fs^2/rad (black spectral phase trace in Fig. 4.A) to account for the fact that the pulse autocorrelation indicates a pulse of approximately 120 fs for a spectrum which is capable of supporting a Fourier-transform pulse duration of 27 fs. The blue trace in Fig. 4.B corresponds to the calculated temporal profile when the π-step is set at the center of the pulse spectrum (960 nm, blue spectral phase trace in Fig. 4.A). This condition corresponds to the largest modulation we can expect from a signal scaling with I^2, as shown in the continuous trace in Fig. 4.C, calculated by integrating the square of the temporal dependence (Fig. 4.B) at each spectral position. This is exactly what is observed for the rhodamine 6G trace in Fig. 4.D (green circles), where the minimum of the fluorescence as a function of the π-step position occurs around this position. We then repeated the procedure in living mice monitoring the B-wave amplitude as a reporter for phase-modulation. The results obtained independently for two mice are shown in Fig. 4.D (red triangles). We observed that the B-wave amplitude obtained from living mice and the fluorescence of Rhodamine 6G upon TPA have the same trend: a decrease when the π -step is located at the center of the spectrum. To highlight the good agreement between the *in vivo* experiment and the theoretical behavior, in Fig. 4.C, we overlapped the experimental trace obtained on mouse 1 with the calculated spectral response.

4. Conclusion

We performed a comprehensive study of the visual process generated by TPA. The ERG response upon infrared excitation is sensitive to the pulse duration, beam size and energy. Interestingly, the dependence on pulse duration and energy follows the trend set by the I^2 dependence of TPA, while the behavior for diam-

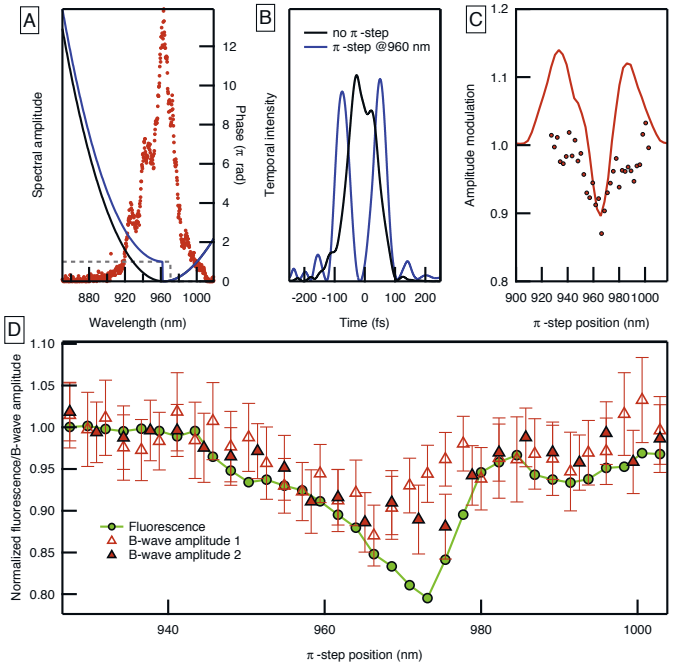

Fig. 4. π-step experimental results and simulations. A: Measured spectrum (red dots), spectral phase representations of a positive linear chirp of 1200 fs2/rad with (blue) and without (black) π-step at 960 nm. B: Calculated temporal intensity as a function of time for chirped pulses with a π-step at 960 nm (blue line) and without π-step (black line). C: Calculated amplitude modulation for different π-step positions (red lines). Normalized B-wave amplitude of mouse 1 (red dots). D: B-wave amplitude obtained on two different mice (red triangles) and by fluorescence on Rhodamine 6G in ethanol (green circle) as a function of the π-phase step spectral position.

eter is different, pointing towards the interplay of a short-term photodynamic process (absorption by the rhodopsin and photoisomerization) and a longer term physiological modulation of the visual response. We demonstrated the acquisition of ERG signals by TPA on living mice. In this context, we showed it is possible to perform spectral-phase shaping of the infrared beam to control the amplitude of the generated B-wave.

Acknowledgments

We acknowledge M. Moret, V. P. Jungo, and J.-M. Matter for invaluable help and the technical support. This work was supported by the SNSF (Swiss National Science Foundation) under Sinergia grant number CRSII5 170981 and the NCCR-MUST (Molecular Ultrafast Science and Technology).

Disclosures. The authors declare no conflicts of interest.

Data availability. Data underlying the results presented in this paper are not publicly available at this time but may be obtained from the authors upon reasonable request.

Animal experiments. Mice were housed and handled in accordance with the guidelines and regulations of the institution and of the state of Geneva (authorization number 29604). C57BL/6 male mice were purchased from Charles River Laboratories.

Received: May 20, 2022

[1] Dario Polli, Piero Altoè, Oliver Weingart, Katelyn M. Spillane, Cristian Manzoni, Daniele Brida, Gaia Tomasello, Giorgio Orlandi, Philipp Kukura, Richard A. Mathies, Marco Garavelli, Giulio Cerullo, *Nature* **2010**, *467.7314*, pp. 440, https://doi.org/10.1038/nature09346.

[2] Helga Kolb, Eduardo Fernandez, and Ralph Nelson, eds. Webvision: The Organization of the Retina and Visual System. Salt Lake City (UT): University of Utah Health Sciences Center, **1995**. https://webvision.med.utah.edu/.

[3] H Kandori, Y Shichida, and T Yoshizawa, *Biochem. (Moscow)* **2001**, pp. 1197, https://doi.org/10.1023/A:1013123016803.

[4] Grazyna Palczewska, Frans Vinberg, Patrycjusz Stremplewski, Martin P. Bircher, David Salom, Katarzyna Komar, Jianye Zhang, Michele Cascella, Maciej Wojtkowski, Vladimir J. Kefalov, Krzysztof Palczewski, *Proc. Natl. Acad. Sci.* **2014**, *111.50*, E5445, https://doi.org/10.1073/pnas.1410162111.

[5] Daisuke Kojima, Suguru Mori, Masaki Torii, Akimori Wada, Rika Morishita, Yoshitaka Fukada, *PLoS ONE* **2011**, *6.10*, e26388, https://doi.org/10.1371/journal.pone.0026388.

[6] Geoffrey Gaulier, Quentin Dietschi, Swarnendu Bhattacharyya, Cédric Schmidt, Matteo Montagnese, Adrien Chauvet, Sylvain hermelin, florence Chiodini, Luigi Bonacina, Pedro L. Herrera, Ursula Röthlisberger, Ivan Rodriguez, Jean-Pierre Wolf, *Sci. Adv.* **2021**, *7.18*, eabe1911, https://doi.org/10.1126/sciadv.abe1911.

[7] Yuqian Ma, Jin Bao, Yuanwei Zhang, Zhanjun Li, Xiangyu Zhou, Changlin Wan, Yang Zhao, Gang Han, Tian Xue, *Cell* **2019**, *177.2*, 243. e15, https://doi.org/10.1016/j.cell.2019.01.038.

[8] Frans Vinberg, Grazyna Palczewska, Jianye Zhang, Karazyna Komar, Maciej Wohtkowski, Vladimir J. Kefalov, Krzysztof Palczewski, *Neurosci.* **2019**, *416*, pp. 100, https://doi.org/10.1016/j.neuroscience.2019.07.047.

[9] Marcin J. Marzejon, Łukasz Kornaszewski, Jakub Bogusławski, Piotr Ciąćka, Miłosz Martynow, Grażyna Palczewska, Sebastian Maćkowski, Krzysztof Palczewski, Maciej Wojtkowski, and Katarzyna Komar, *Biomed. Opt. Express* **2021,** *12.1*, pp. 462, https://doi.org/10.1364/BOE.411168.

[10] Silvestre Manzanera, Daniel Sola, Noe Khalifa, and Pablo Artal, *Biomed. Opt. Express* **2020**, *11.10*, pp. 5603, https://doi.org/10.1364/BOE.403695.

[11] Pablo Artal, Silvestre Manzanera, Katarzyna Komar, Adrián Gambín-Regadera, and Maciej Wojtkowski, *Optica* **2017**, *4.12*, pp. 1488, https://doi.org/10.1364/OPTICA.4.001488.

[12] Daniel Ruminski, Grazyna Palczewska, Maciej Nowakowski, Agnieszka Zielińska, Vladimir J. Kefalov, Katarzyna Komar, Krzysztof Palczewski, and Maciej Wojtkowski, *Biomed. Opt. Express* **2019**, *10.9*, pp. 4551, https://doi.org/10.1364/BOE.10.004551.

[13] Agnieszka Zielińska, Piotr Ciąćka, Maciej Szkulmowski, Katarzyna Komar, *Invest. Ophthalmol. Visual Sci.* **2021**, *62.15*, p. 23, https://doi.org/10.1167/iovs.62.15.23.

[14] Giulio Cerullo and Sandro De Silvestri, *Rev. Sci. Instrum.* **2003**, *74.1*, pp. 1, https://doi.org/10.1063/1.1523642.

[15] C. Manzoni and G. Cerullo, *J. Opt.* **2016**, *18.10*, p. 103501, https://doi.org/10.1088/2040-8978/18/10/103501.

[16] Frans Vinberg, Alexander V Kolesnikov, and Vladimir J Kefalov, *Vision Res.* **2014**, *101*, pp. 108, https://doi.org/10.1016/j.visres.2014.06.003.

[17] Xiangtian Zhou, Jing Xie, Meixiao Shen, Jianhua Wang, Liqin Jiang, Jia Qu, Fan Lu, *Vision Res*. **2008**, *48.9*, pp. 1137, https://doi.org/10.1016/j.visres.2008.01.030.

[18] S. Remtulla and P. E. Hallett, *Vision Res*. **1985**, *25.1*, pp. 21, https://doi.org/10.1016/0042-6989(85)90076-8.

[19] Ying Geng, Lee Anne Schery, Robin Sharma, Alfredo Dubra, Kamran Ahmad, Richard T. Libby, and David R. Williams, *Biomed. Opt. Express* **2011**, *2.4*, pp. 717, https://doi.org/10.1364/BOE.2.000717.

[20] M. Anastasi, Brai M., Lauricella M., Geracitano R., *Ophthalmic Res*. **1993**, *25.3*, pp. 145, https://doi.org/10.1159/000267283.

[21] Soile Nymark, H. Heikkinen, C. Haldin, K. Donner, A. Koskelainen, *J. Physiol.* **2005**, *567.3*, pp. 923, https://doi.org/10.1113/jphysiol.2005.090662.

[22] ShannonMSaszik, JohnGRobson, and Laura J Frishman, *J. Physiol*. **2022**, *543.3*, pp. 899, https://doi.org/10.1113/jphysiol.2002.019703.

[23] Gregory S Gilmour, Frédéric Gaillard, Juliane Watson, Sharee Kuny, Silvina C. Mema, Stephan Bonfield, William K. Stell, Yves Sauvé, *Vision Res*. **2008**, *48.27*, pp. 2723, https://doi.org/10.1016/j.visres.2008.09.004.

[24] Sidney M Gospe, Amanda M. Travis, Alexander V. Kolesnikov, Mikael Klingeborn, Luyu Wang, Vladimir J. Kefalov, Vadim Y. Arshavsky, *J. Biol. Chem*. **2019**, *294.33*, pp. 12432, https://doi.org/10.1074/jbc.RA119.007945.

[25] Morven A Cameron, Alun R. Barnard, Roelof A. Hut, Xavier Bonnefont, Gijsbertus T. J. van der Horst, Mark W. Hankins, Robert J. Lucas, *J. Biol. Rhythms,* **2008**, *23.6*, pp. 489, https://doi.org/10.1177/0748730408325874.

[26] Eric R Kandel *et al*. *Principles of neural science*. Vol. 4. McGraw-hill New York, **2000**.

[27] Hiroo Imai, Vladimir Kefalov, Keisuke Sakurai, Osamu Chisaka, Yoshiki Ueda, Akishi Onishi, Takefumi Morizumi, Yingbin Fu, Kazuhisa Ichikawa, Kei Nakatani, Yoshihito Honda, Jeannie Chen, King-Wai Yau, Yoshinori Shichida, *J. Biol. Chem*. **2007**, *282.9*, pp. 6677, https://doi.org/10.1074/jbc.M610086200.

[28] Frans Vinberg and Vladimir Kefalov, *J. Visualized Exp*. **2015**, *JoVE 99*.

[29] Doron Meshulach and Yaron Silberberg, *Physical Rev. A* **1999**, *60.2*, pp. 1287, https://doi.org/10.1103/PhysRevA.60.1287.

[30] Jing Ma, Wenjing Cheng, Shian Zhang, Donghai Feng, Tianqing Jia, Zhenrong Sun, Jianrong Qui, *Laser Phys. Lett*. **2013**, *10.8*, p. 085304, https://doi.org/10.1088/1612-2011/10/8/085304.

[31] Vadim V Lozovoy, Igor Pastirk, Katherine A. Walowicz, Marcos Dantus, *J. Chem. Phys*. **2003**, *118.7*, pp. 3187, https://doi.org/10.1063/1.1531620.

[32] Lev Chuntonov, Avner Fleischer, and Zohar Amitay, *Opt. Express* **2011**, *19.7*, pp. 6865, https://doi.org/10.1364/OE.19.006865.

[33] Andrew M Weiner, *Opt. Commun*. **2011**, *284.15*, pp. 3669, https://doi.org/10.1016/j.optcom.2011.03.084.